doi:10.1093/jmcb/mjab059
Published online September 25, 2021

Article

Membrane dynamics of ATG4B and LC3 in autophagosome formation

Yuanyuan Zhou[1], Zhenkun Wang[1], Yijia Huang[1], Chujie Bai[2], Xianli Zhang[1], Mengdie Fang[3], Zhenyu Ju[1,*], and Bo Liu[1,*]

[1] Key Laboratory of Regenerative Medicine of Ministry of Education, Guangzhou Regenerative Medicine and Health Guangdong Laboratory, Institute of Aging and Regenerative Medicine, Jinan University, Guangzhou 510632, China
[2] Key Laboratory of Carcinogenesis and Translational Research (Ministry of Education/Beijing), Department of Bone and Soft Tissue Tumor, Peking University Cancer Hospital and Institute, Beijing 100142, China
[3] College of Bioengineering, Hangzhou Medical College, Hangzhou 310013, China
* Correspondence to: Bo Liu, E-mail: ydqc_666@126.com; Zhenyu Ju, E-mail: zhenyuju@163.com

Edited by Xuebiao Yao

The biogenesis of autophagosomes provides the basis for macroautophagy to capture and degrade intracellular cargoes. Binding of the autophagy-related protein ATG8/LC3 to autophagic membranes is essential to autophagosome formation, which involves the specific and dynamic processing of ATG8/LC3 by cysteine protease ATG4. However, to date, the mechanism whereby ATG4 is recruited to the membranes, the interaction of ATG4 and ATG8/LC3 on the membranes, and its role in the growth of phagophore are not completely understood. Here, we used fluorescence recovery after photobleaching to monitor the turnover of GFP-tagged ATG4B and LC3B in living animal cells. The data show that ATG4B localizes to early autophagic membranes in an LC3B-dependent manner. During autophagy, ATG4B and LC3B undergo rapid cytosol/isolation membrane exchange but not at the cytosol/completed autophagosome. In addition, ATG4B activity controls the efficiency of autophagosome formation by impacting the membrane binding/dissociation of LC3B. These data suggest that ATG4 and LC3 play interdependent roles in the formation of autophagosomes.

Keywords: autophagy, autophagosome biogenesis, ATG4, LC3, live-cell imaging, membrane binding kinetics

Introduction

Macroautophagy (hereafter, autophagy) is a highly conserved lysosome-mediated intracellular decomposition process in eukaryotic cells, which involves the formation of autophagosomes and concurrent capture of cytoplasmic components (Lamb et al., 2013; Lum et al., 2015; Yu et al., 2018). The biogenesis of autophagosomes begins with the generation from the intracellular membrane system of the isolation membranes that enlarge, elongate, and eventually seal as double-membrane vesicles (Nakatogawa et al., 2007; Lum et al., 2015; Yu et al., 2018). In mammalian cells, this process depends on multiple autophagy-related (ATG) proteins (Walker and Ktistakis, 2020), among which microtubule-associated protein 1 light chain 3 (MAP1LC3/LC3), the ortholog protein of yeast ATG8, is crucial to the growth of the isolation membranes and recognition of autophagic cargoes (Pankiv et al., 2007; Weidberg et al., 2010; Tsuboyama et al., 2016). To perform its role, newly synthesized LC3 undergoes a series of processes, including the cleavage at the carboxyl terminal glycine 120 site by the cysteine protease ATG4 to form LC3-I, conjugation of LC3-I with phosphatidylethanolamine (PE) through a ubiquitylation-like system that generates membrane-bound LC3-II, and ATG4-mediated deconjugation of LC3-II and PE on the membrane (Kabeya et al., 2000; Kirisako et al., 2000; Xie et al., 2008; Mizushima et al., 2011; Abreu et al., 2017).

Among ATG proteins, ATG4 is the only protease that functions in lipidation/delipidation of the ATG8 protein. In mammalian cells, there are four ATG4 homologues (ATG4A, ATG4B, ATG4C, and ATG4D), which own the different processing activity to ATG8 homologues and contribute to autophagy (Agrotis et al., 2019). *In vitro* proteolytic analysis indicates that ATG4B possesses the strongest activity and the broadest spectrum against both LC3-family and GABARAP-family proteins (Li et al.,

Received January 14, 2021. Revised June 6, 2021. Accepted June 7, 2021.

2011; Kauffman et al., 2018). By contrast, ATG4A has only weak activity to GABARAPs, and ATG4C and ATG4D show minimum protease activities with almost all ATG8 homologues (Li et al., 2011; Kauffman et al., 2018). Evidence accumulated from yeast studies has suggested that both lipidation and delipidation of ATG8 are required for efficient autophagosome formation. Nevertheless, although lipidation is clearly essential for targeting ATG8/LC3 to the phagophore assembly site/preautophagosomal structure (PAS), the significance of ATG8/LC3 delipidation is still incompletely elucidated. It was shown that in yeast deficient for ATG4-mediated ATG8 delipidation, ATG8–PE accumulates on various intracellular organelles, which depletes unlipidated ATG8 and thereby attenuates its localization to the PAS (Nair et al., 2012; Nakatogawa et al., 2012; Yu et al., 2012). Recently, it was also proposed that delipidation of ATG8 from PE is dispensable for targeting ATG8 to PAS but is required directly for the growth of phagophores (Hirata et al., 2017), suggesting a potential role of ATG8 delipidation on the isolation membranes. However, at least under optical microscope and in mammals, the localization of ATG4 on autophagic membranes has not been identified. During autophagy, the membrane association of ATG4 and its interaction with ATG8/LC3 proteins on autophagic membranes remain largely unknown.

To study the dynamics of ATG4 and its interaction with ATG8/LC3 during autophagosome formation *in vivo*, in this study, we characterized the membrane binding kinetics of ATG4B and LC3B in living cells. We observed that ATG4B was localized to autophagosomes in LC3B-overexpressing cells in an LC3B-dependent manner. ATG4B and LC3B cycle separately on/off the membranes, and the cycling of LC3B is regulated by ATG4B, which is required for the efficiency of autophagosome formation.

Results

ATG4B is located on autophagic membranes and regulates autophagosome formation

To study the dynamics of ATG4 in animal cells, we first got a GFP-ATG4B plasmid and transfected it into HEK293 cells. By staining endogenous LC3, we found that overexpression of GFP-ATG4B deleted intracellular LC3 puncta in fed and starved cells (Figure 1A; Supplementary Figure S1B), and normal LC3 puncta were observed in cells overexpressing ATG4B^{LIRCM}, an ATG4B variant in which the LC3-interaction region is mutated and fails to interact with LC3 (Supplementary Figure S1A–C; Skytte-Rasmussen et al., 2017). Meanwhile, the conversion of LC3-I to LC3-II in starved cells with or without the lysosome inhibitor chloroquine (CQ) was dramatically suppressed by GFP-ATG4B overexpression (Figure 1B). In these cells, GFP-ATG4B showed a diffuse distribution in the cytoplasm (Figure 1A). These observations are consistent with the previous study (Fujita et al., 2008a) indicating that excess ATG4B inhibits the membrane association of LC3B. However, interestingly, when mCherry-LC3B was coexpressed with GFP-ATG4B in HEK293 cells, under cell starvation, these cells were able to form mCherry-LC3B puncta, and GFP-ATG4B was associated with these puncta demonstrating colocalization with mCherry-LC3B (Figure 1C). At the same time, mCherry-LC3B-II and endogenous LC3B-II were produced in these cells (Figure 1D). Next, we treated the cells with the class III PtdIns3K inhibitor 3-methyladenine (3-MA) to suppress autophagy under starvation conditions. The addition of 3-MA significantly inhibited the formation of mCherry-LC3B puncta and GFP-ATG4B puncta (Figure 1E). In addition, in starved *Atg5*-knockout mouse embryonic fibroblasts (MEF; an autophagy-deficient cell), the puncta of mCherry-LC3B and GFP-ATG4B were also dramatically abolished (Figure 1F). Therefore, the produced mCherry-LC3B puncta and mCherry-LC3B-II/LC3B-II represented an increase in autophagosome formation. Together, these results suggest that the relative ratio of intracellular ATG4B to LC3B impacts the efficiency of LC3B lipidation and autophagosome formation.

LC3-dependent association of ATG4B with autophagic membranes

Taking advantage of ATG4B being observed on autophagic membranes in LC3B-overexpressing cells, we then wanted to know when and how ATG4B is recruited to these membranes. We checked the colocalization of ATG4B with marker proteins representing different autophagy steps in cells stably overexpressing LC3B. Under cell starvation, ATG4B colocalized with the punctate structures of ULK1, DFCP1, ATG16, and STX17 where LC3B was contained (Figure 2A–D). Interestingly, ATG4B was not localized to LAMP1/LC3B-positive puncta (Figure 2E). Meanwhile, when the puncta of LC3B and ATG4B were abolished in the starved *Atg5*-knockout cells, the colocalization of ATG4B with ULK1 or DFCP1 also disappeared (Supplementary Figure S2A and B). Together, these observations suggest that ATG4B binds to autophagic membranes following LC3B and is no longer associated with these membranes after autophagosome–lysosome fusion.

To confirm that the membrane binding of ATG4B is dependent on LC3, we observed the distribution of ATG4B^{LIRCM}, an ATG4B mutation that fails to interact with LC3, in cells coexpressing GFP-ATG4B^{LIRCM} and mCherry-LC3B. Under cell starvation, GFP-ATG4B^{LIRCM} was unable to localize to mCherry-LC3B puncta but diffused in the cytoplasm (Figure 2F). Taken together, these data suggest that during autophagosome formation, ATG4B is associated with autophagic membranes in an LC3-dependent manner.

LC3 cycles on/off membranes but not complete autophagosomes or autolysosomes

Accumulated evidence obtained from yeast and mammalian cells suggest that the association of ATG8 with PAS or LC3 with the isolation membrane is a dynamic process (Xie et al., 2008; Koyama-Honda et al., 2013; Karanasios and Ktistakis, 2015; Tsuboyama et al., 2016). The results of living cell imaging showed that during autophagosome formation, the total

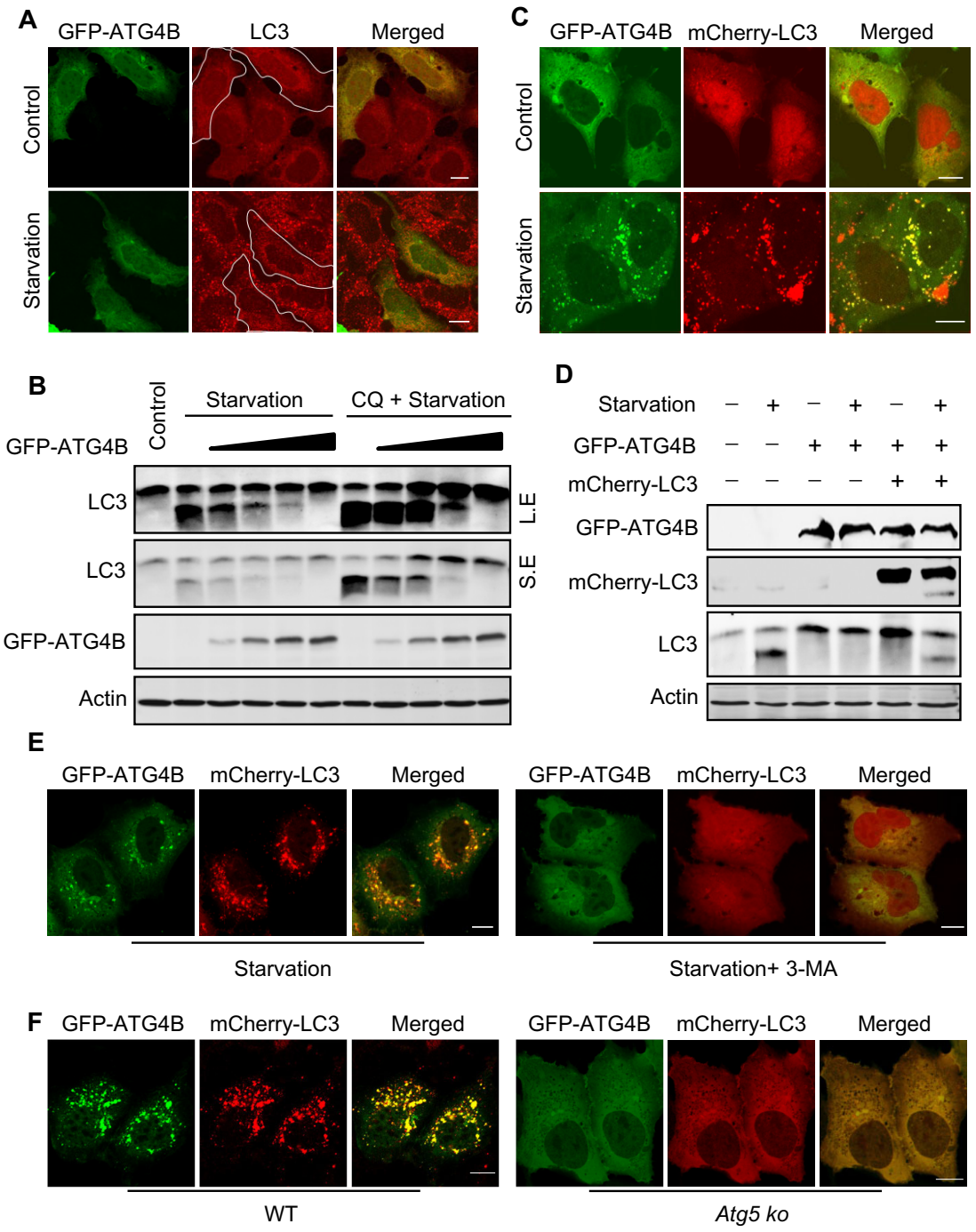

Figure 1 Characterization of autophagosome formation in ATG4B-overexpressing cells. (**A**) Formation of LC3 puncta in ATG4B-overexpressing cells with or without starvation. The cells were stained with a specific anti-LC3 antibody and visualized with confocal microscopy. (**B**) Western blotting analysis of LC3-II production in the starved cells expressing different levels of GFP-ATG4B in the presence or absence of CQ. LE, long exposure; SE, short exposure. (**C**) Formation of GFP-ATG4B and mCherry-LC3B puncta in the GFP-ATG4B and mCherry-LC3B coexpressing cells treated with or without starvation. (**D**) Western blotting analysis of LC3-II production in the cells only expressing GFP-ATG4B or coexpressing GFP-ATG4B and mCherry-LC3B with or without starvation. (**E**) Formation of GFP-ATG4B and mCherry-LC3B puncta in the mCherry-LC3B and GFP-ATG4B coexpressing cells treated with starvation or starvation and 3-MA. (**F**) Formation of GFP-ATG4B and mCherry-LC3B puncta in the starved *Atg5*-knockout MEF coexpressing mCherry-LC3B and GFP-ATG4B. Scale bar, 10 μm.

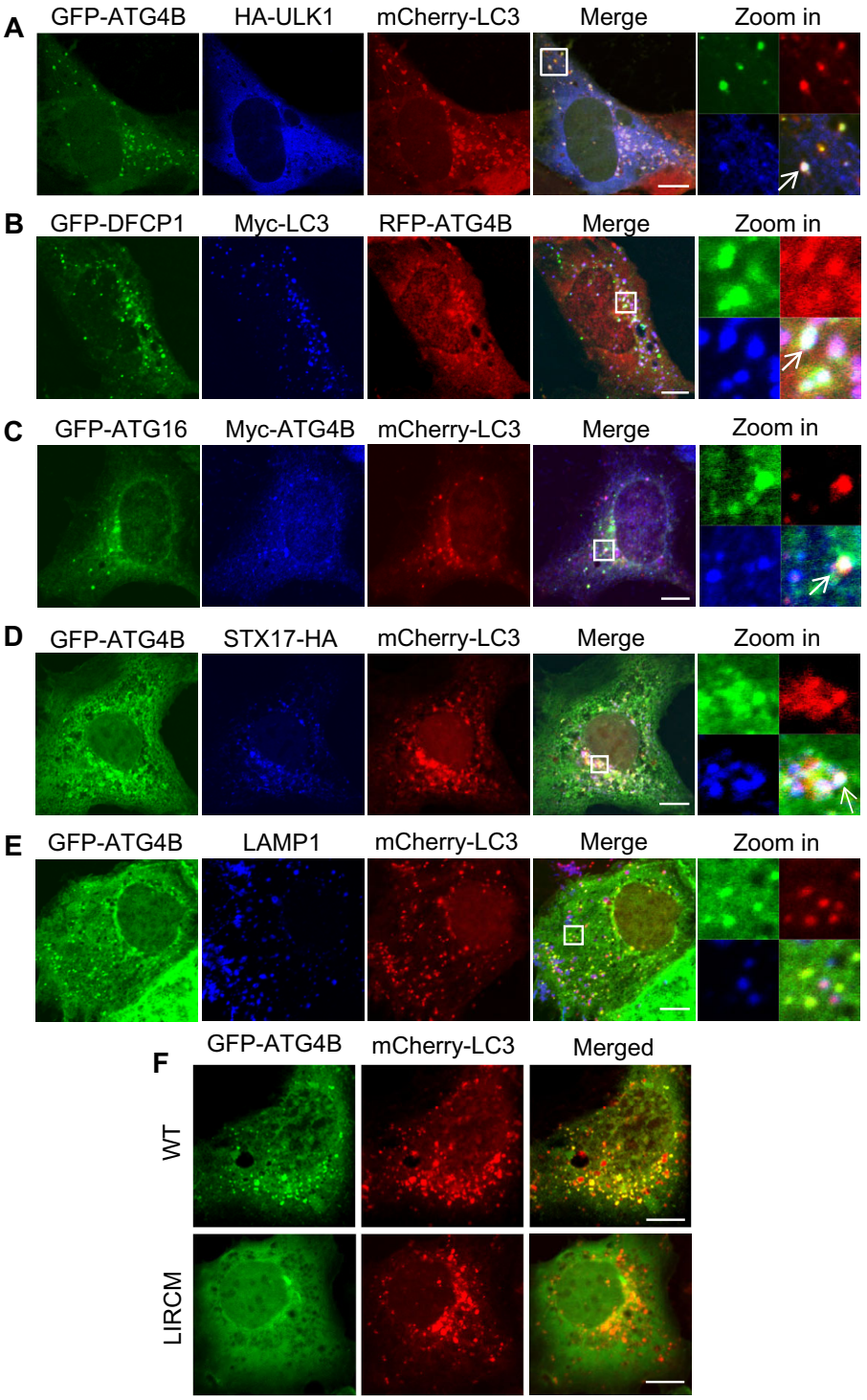

Figure 2 Association of ATG4B with the autophagic membranes. (**A**–**E**) Localization of ATG4B with HA-ULK1 (**A**), GFP-DFCP1 (**B**), GFP-ATG16 (**C**), STX17-HA (**D**), or LAMP1 (**E**) in the starved cells. (**F**) Images of mCherry-LC3B and GFP-ATG4B in the starved cells coexpressing mCherry-LC3B and GFP-ATG4B or GFP-ATG4B^{LIRCM}. Scale bar, 10 μm.

intensity of the ATG8/LC3 signal on the PAS/isolation membrane increased gradually, peaked in ~6 min, and then began to decline (Xie et al., 2008; Koyama-Honda et al., 2013; Tsuboyama et al., 2016). While these indicate a continued recruitment of ATG8/LC3, it is not clear whether these proteins are stably associated or undergo multiple cycles. To address this, we measured the kinetic properties of GFP-LC3B on/off membranes by carrying out fluorescence recovery after photobleaching (FRAP) experiments in living cells. Rapid recovery of the GFP-LC3B signal was observed after photobleaching GFP

fluorescence in GFP-LC3B dots (the recovery half-time $t_{1/2} \approx 40$ sec), indicating a sustained membrane binding of LC3 from the cytosolic pool (Figure 3A and F). Nevertheless, when we assessed the turnover of the photoactivatable GFP-tagged LC3B (PAGFP-LC3B) after photoactivation of the PAGFP-LC3B dots, we detected a continued decrease of the PAGFP-LC3B signal over time (Figure 3B and G), suggesting a continued dissociation of LC3 from autophagic membranes.

It has been reported that STX17 is recruited to closure autophagosomes (Tsuboyama et al., 2016). Interestingly, in cells coexpressing GFP-LC3B and LAMP1-RFP or STX17-mCherry, with FRAP, we found that GFP-LC3B fluorescence on LAMP1-RFP-positive (Figure 3C and F) or STX17-mCherry-positive (Figure 3D and F) puncta was not able to recover at all after photobleaching. The turnover of photoactivated PAGFP-LC3B on LAMP1-RFP-positive puncta was also dramatically suppressed (Figure 3E and G). The results suggest that LC3B can no longer be recruited onto completed autophagosomes or autolysosomes.

Membrane association–dissociation cycle of ATG4B

We then addressed whether ATG4B resides stably or only transiently after being recruited to autophagic membranes. In cells stably expressing Myc-LC3B, transfected GFP-ATG4B was presented on punctate structures upon cell starvation, as observed in cells overexpressing mCherry-LC3B. With FRAP, we observed a rapid recovery of the GFP-ATG4B signal after photobleaching the GFP-ATG4B puncta ($t_{1/2} \approx 12$ sec), indicating a continued recruitment of cytosolic GFP-ATG4B to autophagosomes (Figure 4A). To further confirm the recruitment of ATG4B to autophagosomes, we tracked GFP-ATG4B fluorescence on the mCherry-LC3B puncta by time-lapse confocal microscopy. We found that with the growth of mCherry-LC3B puncta, the GFP-ATG4B signal was also increased on the puncta (Figure 4B), confirming the continuous recruitment of ATG4B to the growing autophagic membrane. We next examined whether GFP-ATG4B on autophagosomes goes through continued dissociation from the membranes by using fluorescence loss in photobleaching (FLIP). Under cell starvation conditions, accompanying with repeated photobleaching of GFP-ATG4B in a region of cytoplasm, virtually the autophagosome-associated GFP-ATG4B fluorescence was lost over time (Figure 4C and E). These results suggest that similar to LC3B, ATG4B undergoes dynamic cycling on and off autophagosomal membranes during autophagosome formation. Interestingly, in GFP-ATG4B and STX17-mCherry-cotransfected Myc-LC3B stable cells, when we performed FRAP experiments onto GFP-ATG4B puncta, which were positive with STX17-mCherry, no GFP-ATG4B fluorescence recovery was observed after photobleaching (Figure 4D and F), suggesting that similar to LC3, ATG4B is no longer recruited to complete autophagosomes.

ATG4B regulates the cycling of LC3 and the efficiency of autophagosome formation

Because ATG8–PE and autophagosomes are not formed in ATG4-deleted cells (Nakatogawa et al., 2012), to investigate the role of ATG4 in regulating the membrane cycling of LC3, we used ATG4B-knockdown cells in which, consistently with the previous study, the LC3 lipidation and autophagosome formation could still be induced by cell starvation (Figure 5A; Supplementary Figure S3; Yoshimura et al., 2006). Compared with control cells, short-time (1 h) starvation only stimulated the cells expressing ATG4B ShRNA to form a few LC3 puncta (Figure 5A and B). However, with prolonged cell starvation (4 h), equivalent LC3 puncta were observed in these cells (Figure 5A and B). With the use of Tioconazole (TC), an ATG4 inhibitor that suppresses ATG4 protease activity (Liu et al., 2018), a similar effect on the formation of LC3 puncta was observed (Figure 5C and D), suggesting a slower autophagosome formation induced by ATG4B inhibition.

To test whether the slowered autophagosome formation in ATG4B-knockdown cells is due to an impaired membrane cycling of LC3, we performed FRAP experiments on GFP-LC3B puncta in cells coexpressing ATG4B ShRNA. We found that compared with control cells, the recovery of GFP-LC3B fluorescence was significantly inhibited after photobleaching in ATG4B-knockdown cells (Figure 5E and F). A similar inhibition was also observed in GFP-LC3B-expressing cells treated with TC (Figure 5G and H). Taken together, these data suggest that ATG4B impacts the membrane cycling of LC3B.

Discussion

In this study, our data show that during autophagy, LC3 and ATG4 are constantly and, respectively, cycling on/off growing autophagic membranes but not complete autophagosomes or autolysosomes. The protease activity of ATG4 regulates the efficiency of autophagosome formation by influencing the membrane cycling of LC3 (Figure 6).

To date, the functions of LC3 on autophagosomes for autophagosome closure (Fujita et al., 2008a), autophagosome–lysosome fusion (Nguyen et al., 2016), and inner autophagosomal membrane degradation (Tsuboyama et al., 2016) have been extensively investigated. However, how LC3 dynamically associates with the autophagic membranes during autophagy is still not completely understood. Two different models could be proposed: (i) during autophagosome biogenesis, LC3 is repeatedly associated and disassociated with autophagic membranes; (ii) LC3 is constantly recruited to the membranes and anchored on the membranes until autolysosome formation is complete. In this study, on autophagosome but not autolysosome, the rapid fluorescence recovery of the GFP-LC3B puncta in FRAP (LC3 associated with autophagic membranes, Figure 3A), the fluorescence loss of the PAGFP-LC3B puncta in living images (LC3 dissociation with autophagic membranes, Figure 3B), and the continuous recruitment of ATG4B to the growing autophagic membrane (Figure 4B) suggest a continuous association and dissociation of LC3 on the growing autophagic membranes during autophagosome formation. However, the kinetics of the GFP-LC3B puncta in FRAP (Figure 3F) indicate that even with a longer observation time

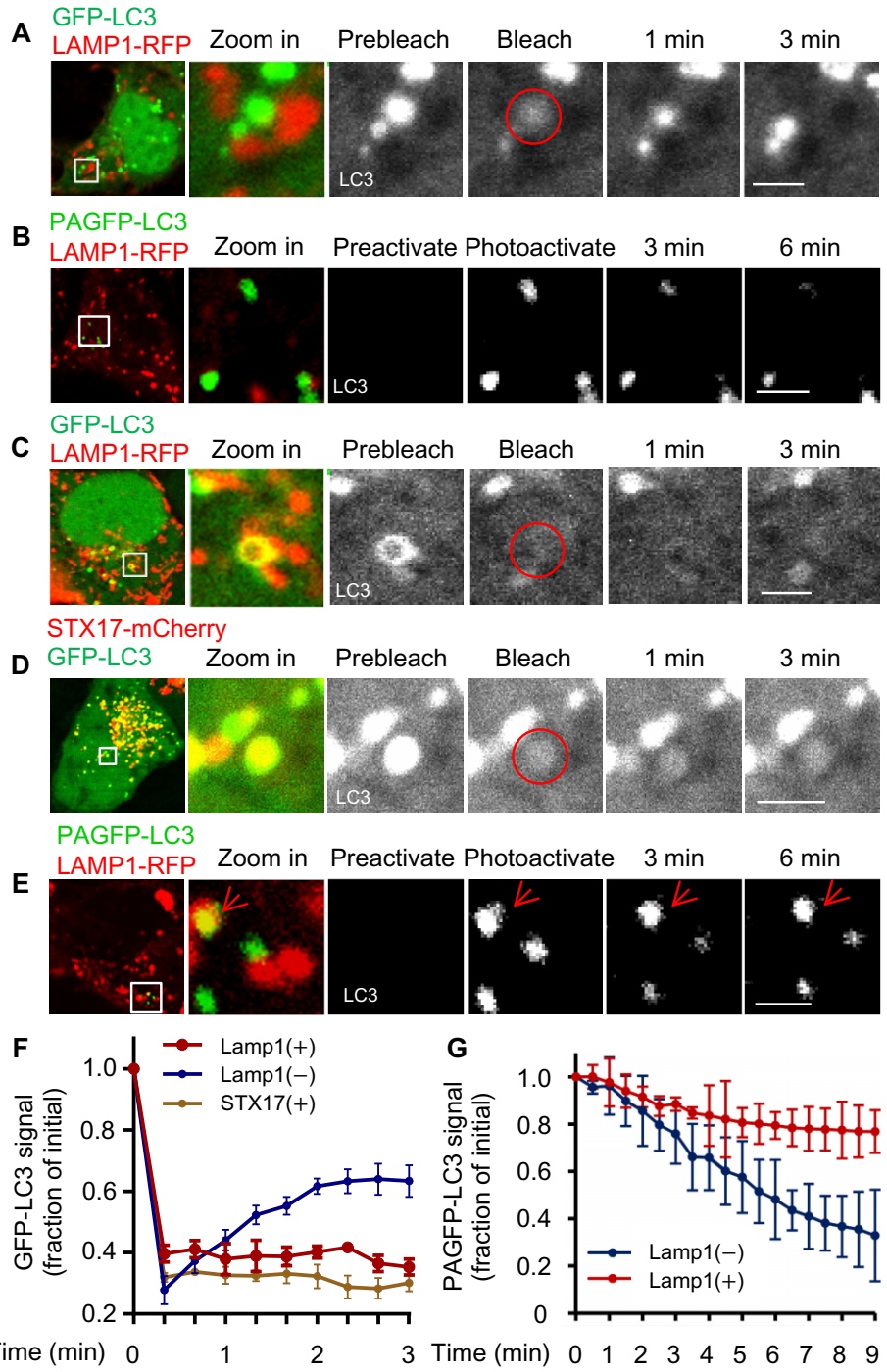

Figure 3 Characterization of the LC3 cycling on/off the autophagic membrane. (**A** and **C**) The starved HEK293 cells coexpressing GFP-LC3B and LAMP1-RFP were imaged before and after photobleaching the indicated GFP-LC3B puncta (red circle region) negative with LAMP1-RFP (**A**) or positive with LAMP1-RFP (**C**) by high-intensity 488-nm laser light. Note the GFP-LC3B fluorescence recovery in the photobleached region. (**B** and **E**) The HEK293 cells coexpressing PAGFP-LC3B and LAMP1-RFP were starved with CQ and imaged with low levels of 488-nm laser light before and after irradiation of the selected region (outlined in white) with 405-nm light. Note the PAGFP fluorescence loss on the PAGFP-LC3B puncta negative with LAMP1-RFP (**B**) or positive with LAMP1-RFP (**E**) with the time lapse. (**D**) The starved cells coexpressing GFP-LC3B and STX17-mCherry were imaged before and after photobleaching the indicated GFP-LC3 puncta (red circle region) by high-intensity 488-nm laser light. Note the GFP-LC3 fluorescence recovery in the photobleached region. (**F**) The GFP-LC3B fluorescence recoveries on the puncta in **A**, **C**, and **D** were quantitatively analyzed. (**G**) The PAGFP-LC3B fluorescence losses on the puncta negative or positive with LAMP1-RFP in **B** and **E** were quantitatively analyzed. Data are presented as mean ± SEM, $n = 5$. Scale bar, 2 μm.

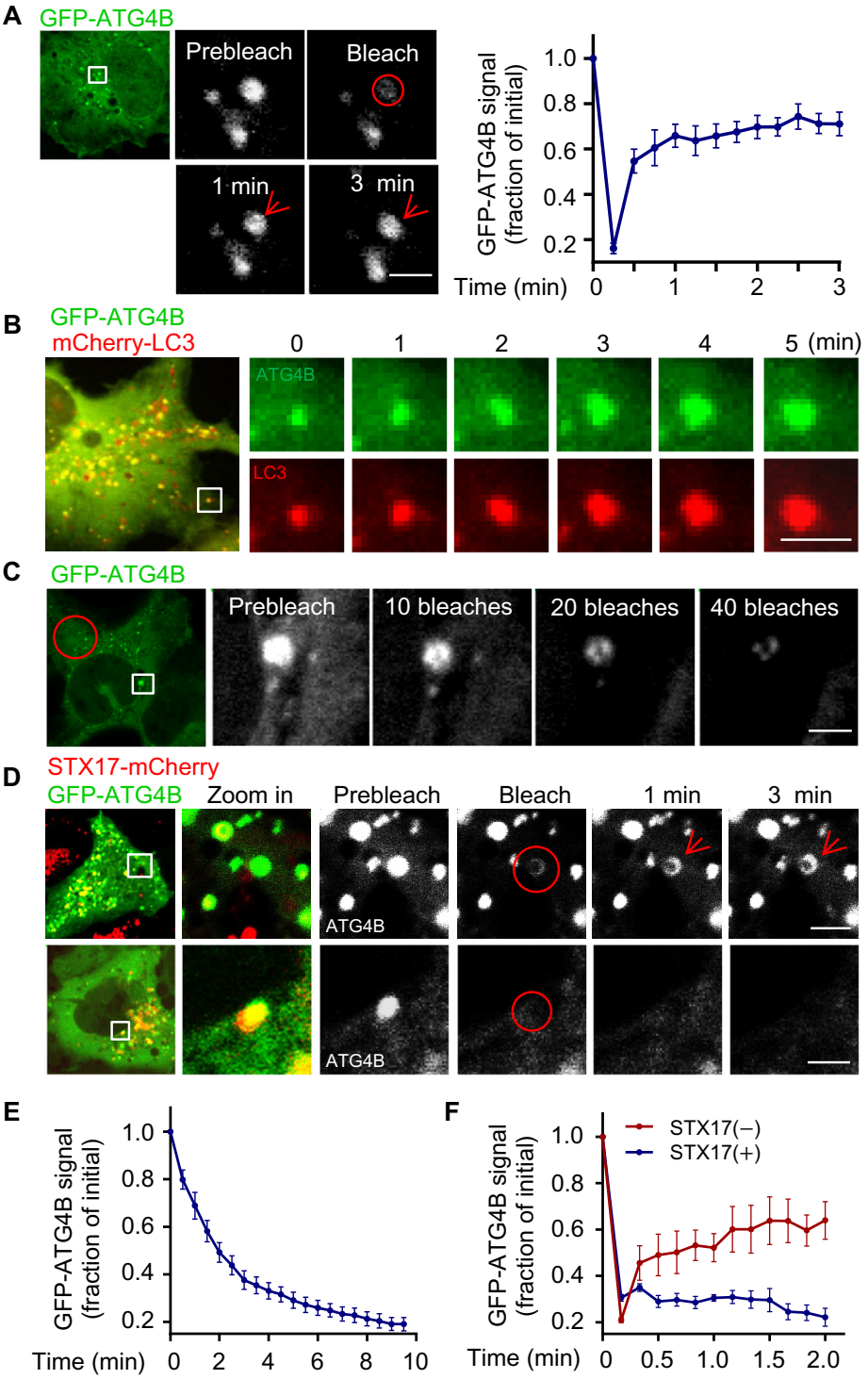

Figure 4 ATG4B is cycling on/off the autophagic membrane. (**A**) The Myc-LC3B-expressing HEK293 cells transfected with GFP-ATG4B were starved and imaged before and after photobleaching the indicated puncta region (red circles) by high-intensity 488-nm laser light. Note the GFP fluorescence recovery in the photobleached region. Quantification shown on the right represents the fluorescence recovery of the GFP-ATG4B signals on the puncta. Data are presented as mean ± SEM, $n = 5$. (**B**) Time-lapse images of GFP-ATG4B and mCherry-LC3B in the starved cells coexpressing GFP-ATG4B and mCherry-LC3B. (**C**) Repeated photobleaching of a cytoplasmic region (red circles) led to the fluorescence loss of GFP-ATG4B puncta in the cells coexpressing GFP-ATG4B and Myc-LC3B with starvation. (**D**) The Myc-LC3B-expressing cells cotransfected with GFP-ATG4B and STX17-mCherry were starved and imaged before and after photobleaching the indicated GFP-ATG4B puncta (red circles) negative or positive with STX17-mCherry by high-intensity 488-nm laser light. (**E** and **F**) Quantification of the fluorescence signals of GFP-ATG4B on the GFP-ATG4B puncta in **C** and **D**. Data are presented as mean ± SEM, $n = 5$. Scale bar, 2 µm.

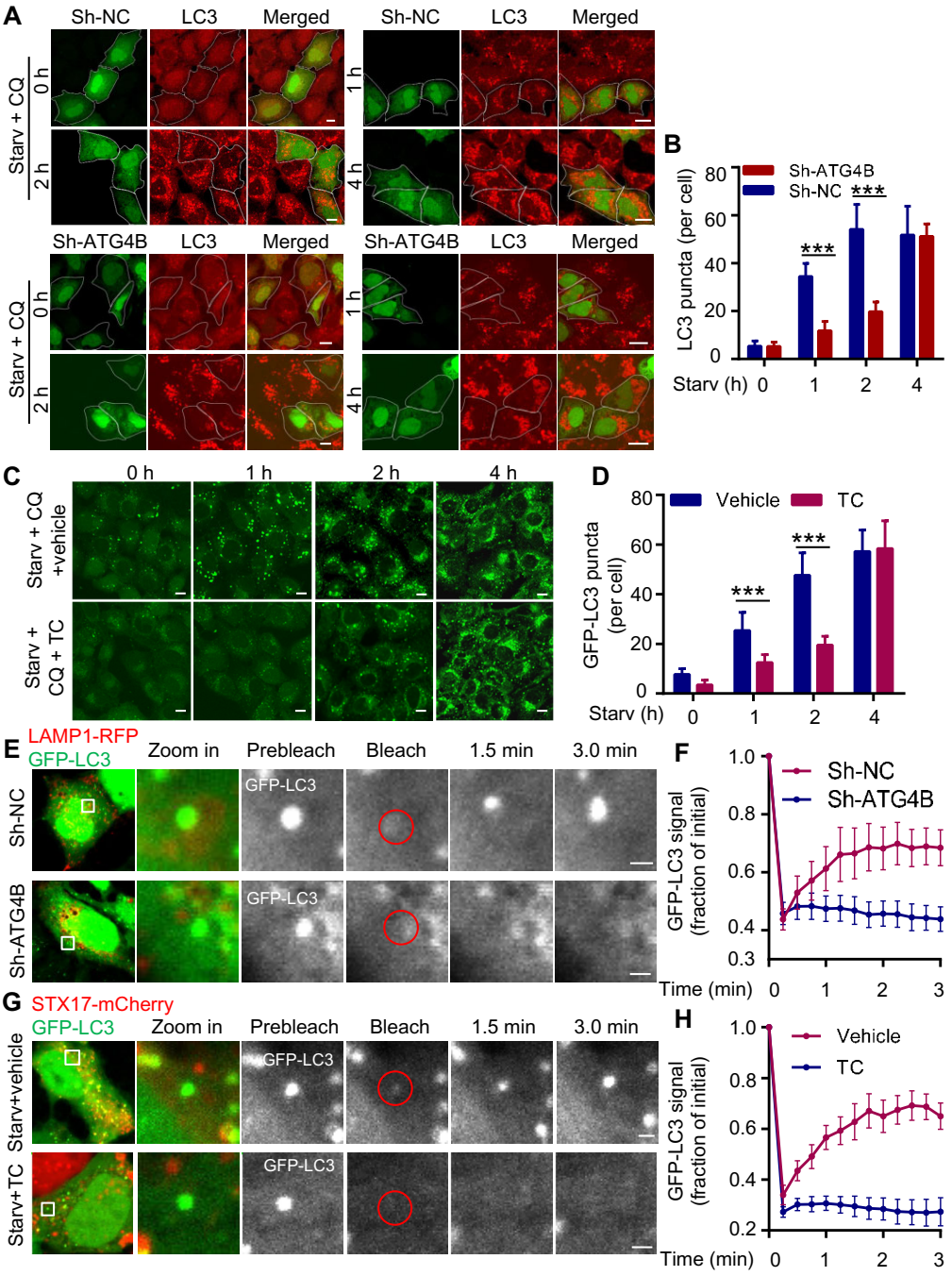

Figure 5 ATG4B regulates the cycling of LC3 and the efficiency of autophagosome formation. (**A**) Formation of LC3 puncta in the control (Sh-NC) or ATG4B-knockdown (Sh-ATG4B) cells (GFP marked) treated with starvation and CQ for the indicated periods. Scale bar, 10 μm. (**B**) Statistical analysis of the number of LC3 puncta per cell in **A**. $n = 15$ cells. (**C**) Formation of GFP-LC3B puncta in the cells stably expressing GFP-LC3B treated with starvation and CQ for the indicated periods in the presence or absence of Tioconazole (TC). Scale bar, 10 μm. (**D**) Statistical analysis of the number of LC3 puncta per cell in **C**. $n = 30$ cells. (**E**) The control or ATG4B-knockdown cells coexpressing GFP-LC3B and LAMP1-RFP were starved and imaged before and after photobleaching the indicated GFP-LC3B puncta negative with LAMP1-RFP (red circles) by high-intensity 488-nm laser light. Note the GFP-LC3B fluorescence recovery in the photobleached region. Scale bar, 1 μm. (**F**) The GFP-LC3B fluorescence recoveries on the GFP-LC3B puncta in **E** were quantitatively analyzed ($n = 5$). (**G**) The starved cells coexpressing GFP-LC3B and STX17-mCherry were treated without or with TC and imaged before and after photobleaching the indicated GFP-LC3B puncta negative with STX17-mCherry (red circles) by high-intensity 488-nm light. Note the fluorescence recovery in the photobleached region. Scale bar, 1 μm. (**H**) The GFP-LC3B fluorescence recoveries on the GFP-LC3B puncta in **G** were quantitatively analyzed ($n = 5$). All the quantitative data are presented as mean ± SEM, $^{***}P < 0.001$.

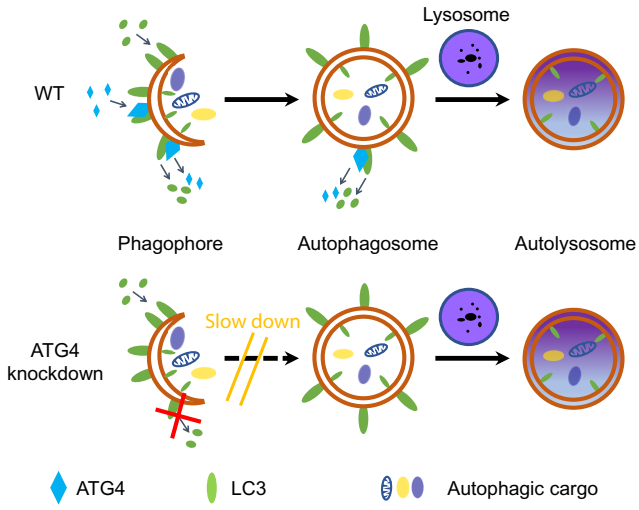

Figure 6 Schematic model for the dynamics of ATG4 and LC3 during autophagosome formation. Both LC3 and ATG4 are cycling on/off the growing autophagic membranes but not complete autophagosomes or autolysosomes. ATG4 regulates the efficiency of autophagosome formation by influencing the membrane cycling of LC3.

postphotobleaching, the signal of GFP-LC3B could not be restored to the prebleaching level, suggesting that after being recruited, a part of LC3 may stably associate with the autophagic membrane and do not undergo cycling, which leads to the finally incomplete fluorescence recovery of the GFP-LC3B puncta after photobleaching. Therefore, taken together, our data suggest that during autophagosome formation, LC3 dynamically associates with autophagic membranes in a mixed pattern: on the growing autophagosome, some LC3 can repeatedly undergo rapid cytosol/membrane exchange, and some LC3 may anchor on membranes to fasten the autophagic cargo until autolysosome formation is completed.

STX17 is negative at elongating isolation membranes and is recruited to the closure autophagosome (Itakura et al., 2012; Tsuboyama et al., 2016). It has been reported that the ATG5–ATG12–ATG16 complex plays an important role in the recruitment of LC3 to autophagosomes (Fujita et al., 2008b). Interestingly, Noboru Mizushima's data show that the ATG5–ATG12–ATG16 complex was released before the completion of autophagosomes (an STX17-positive membrane) (Tsuboyama et al., 2016). Consistently, in this study, no recovery of GFP-LC3B and GFP-ATG4B were observed on autophagic membranes positive with STX17-mCherry in the FRAP experiments (Figures 3D and 4D), suggesting that LC3 and ATG4 can no longer be recruited onto the complete autophagosomes. But the locations of ATG4B and LC3B on the STX17-positive autophagic membranes (Figures 2D, 3D, and 4D) suggest that a few LC3 could still attach at the outer membrane of the complete autophagosome, and a continuous delipidation of LC3 is executed by ATG4 until the successful formation of autolysosome. This possibility is supported by the previous study, which reports a role of LC3 in autophagosome–lysosome fusion (Nguyen et al., 2016). After autolysosome formation, LC3 may completely get off the outer membrane of the autolysosome, and no ATG4B can be observed on the autolysosome. In addition, we found that on few STX17-negative puncta (data not shown), the fluorescence recovery of GFP-LC3B and GFP-ATG4B in the FRAP experiments was also occasionally inhibited, suggesting that autophagosome formation maybe completed before the STX17 recruitment. Meanwhile, besides LC3 and ATG4B, a rapid recovery of GFP-ULK1 and GFP-DFCP1 signals, but not GFP-ATG16 or GFP-STX17 signals, was observed after photobleaching the GFP fluorescence on the autophagic proteins dots (Supplementary Figure S4). These data suggest a different manner of recruitment for the autophagic proteins on the autophagic membrane during autophagy.

After autophagosome–lysosome fusion, the outer membrane of the autophagosome is fused with lysosome, and the inner membrane of the autophagosome is enclosed into lysosome for degradation (Itakura et al., 2012; Tsuboyama et al., 2016). Here, our data show an LC3-dependent association of ATG4B with the early autophagic membranes during autophagosome formation, but no ATG4B was observed on the membranes after autophagosome–lysosome fusion (Figure 2A–E). These results imply that ATG4B may not associate with the inner membrane of autophagosome and could not interact with LC3 localized at the inner membrane of autophagosome. One of the most likely reasons is that the combination of LC3 with the autophagic cargo blocks the interaction of ATG4B with LC3 at the inner membrane of autophagosome, which may also result in a stably binding of LC3 at autophagosomal inner membrane to fix the autophagic cargo. Another possibility might be the sunken curvature of the autophagosomal inner membrane, which may lead a stronger stereospecific blockade for the interaction of ATG4B and LC3 at the inner surface of the autophagic membrane. In addition, although we found that ATG4B localizes to the autophagosome by interacting with LC3, the kinetics of GFP-LC3B and GFP-ATG4B on autophagosome in FRAP show that the recovery of ATG4B is much faster than that of LC3 ($t_{1/2}$: 12 sec vs. 40 sec), suggesting that recruitments of ATG4B and LC3 to the autophagosome are in different manners.

Materials and methods

Cell cultures and transfection

HEK293 cells were cultured in Dulbecco's modified Eagle medium with 10% fetal bovine serum at 37°C under 5% CO_2. Transient transfection was performed using Lipofectamine 3000/2000 according to the manufacturer's instructions. Cells stably expressing GFP-LC3B, Myc-LC3B, or mCherry-LC3B were created by transient transfection followed by selection with G418 (500 μg/ml). Cells coexpressing LC3B with other proteins were created by transient transfecting the protein into the LC3B stable cell line. ATG4B-knockdown cells were created by transient transfecting ATG4B ShRNA targeted to the sequence GAAGCTTGCTGTCTTCGAT followed by selection with G418.

Reagents, antibodies, and plasmids

Chloroquine, 3-methyladenine, G418 were obtained from Sigma. Tioconazole was obtained from Selleck. The following

antibodies were used: anti-GFP (Santa Cruz, sc9996), anti-LC3 (Sigma, L7643), anti-ATG4B (Sigma, A2981), anti-actin (Sigma, A5316), anti-LAMP1 (Santa Cruz, sc20011), anti-HA (Santa Cruz, sc7392), and anti-Myc (Santa Cruz, SC-40). GFP-LC3B, mCherry-LC3B, Myc-LC3B, PAGFP-LC3B, GFP-DFCP1, and HA-ULK1 have been described previously (Huang et al., 2015; Wan et al., 2018; You et al., 2019). GFP-ATG4B was a gift from Zvulun Elazar (Department of Biological Chemistry, The Weizmann Institute of Science, Israel) (Scherz-Shouval et al., 2007). RFP-ATG4B and GFP-ATG4B^{LIRCM} were made by, respectively, cloning the corresponding ATG4B DNA fragments into the pmRFP-C1 and pEGFP-C1 vectors using *Eco*RI and *Bam*HI restriction sites. GFP-ATG16 and STX17 cDNA were gifts from Yingyu Chen (Peking University School of Basic Medical Science, China). LAMP1-RFP was generated by cloning the corresponding cDNA fragments into the pmRFP-N1 vector using *Eco*RI and *Bam*HI restriction sites. mCherry-STX17 and STX17-GFP were made by cloning the corresponding STX17 cDNA fragments into the pmCherry-C1 and pEGFP-N1 vectors using *Kpn*I and *Bam*HI restriction sites.

Autophagy induction

Cells were washed three times with prewarmed phosphate-buffered saline (PBS) and then incubated in starvation medium (1% bovine serum album, 1 mM $CaCl_2$, 150 mM NaCl, 1 mM $MgCl_2$, 5 mM glucose, and 20 mM HEPES, pH 7.4) at 37°C for 1–4 h.

Western blotting and immunoprecipitation

For immunoprecipitation, cells were lysed with Nonidet P40 lysis buffer (50 mM Tris–HCl, pH 7.5, 1 mM EDTA, 100 mM NaCl, 1% NP-40, 10% glycerol, and 1 mM dithiothreitol) containing protease inhibitors. After centrifugation, the supernatants were incubated overnight with antibodies followed by incubation with Protein A/G agarose for 2 h at 4°C. Immunocomplexes were washed and analyzed by western blotting, which was performed as described previously (Liu et al., 2014).

Immunostaining and confocal microscopy

For immunostaining, cells were cultured on coverslips and fixed in 4% formaldehyde. After washing twice with PBS, the cells were incubated in PBS (pH 7.4) containing 10% fetal calf serum (PBS/FCS) to block nonspecific sites of antibody adsorption. Then, the cells were incubated with appropriate primary and secondary antibodies in PBS/FCS buffer with 0.1% saponin as indicated in the figure legends. Images were captured with a Zeiss LSM510 Meta or LSM880 laser scanning confocal microscope (Carl Zeiss) with a 63× Plan Apochromat 1.4 NA objective.

For live-cell imaging, cells were cultured in chambers and imaged on a live-cell station. Photobleaching was performed using an appropriate laser line at full power. In FLIP analysis, a selected region was repetitively photobleached, and the loss of fluorescence from regions outside the photobleached region was monitored at low intensity illumination. For the FRAP analysis, a selected region of the cell was photobleached, and the fluorescence recovery of the region was monitored. The recovery half-time ($t_{1/2}$) was measured from the FRAP curve. All the FLIP and FRAP analyses were repeated at least five times in different cells. For quantification of fluorescence intensity, nonsaturated images were taken with a fully open pinhole, whereas nonquantitative images were obtained with a pinhole diameter equivalent to 1–2.5 Airy units.

Statistical analysis

All the statistical data are presented as mean ± SEM. Statistical significance of the differences was determined using Student's *t*-test. Differences were considered significant at values of $P < 0.05$.

Supplementary material

Supplementary material is available at *Journal of Molecular Cell Biology* online.

Acknowledgements

We thank Dr Zvulun Elazar (Department of Biological Chemistry, The Weizmann Institute of Science, Israel) and Dr Yingyu Chen (Peking University School of Basic Medical Science, China) for sharing plasmids.

Funding

This work was supported by the National Natural Science Foundation of China (31671434, 31701203, 81420108017, 81525010, and 91749203), the National Key Research and Development Program of China (2016YFA0100602, 2017YFA0103302, 2020YFA0112404, and 2018YFC2000705), the Program for Guangdong Introducing Innovative and Entrepreneurial Teams (2017ZT07S347), and the Fundamental Research Funds for the Central Universities (21617336).

Conflict of interest: none declared.

Author contributions: B.L. designed the study and wrote the paper. B.L., Y.Z., Z.W., Y.H., and M.F. performed experiments and analyzed data. C.B. and X.Z. provided additional expertise. B.L. and Z.J. supervised the study.

References

Abreu, S., Kriegenburg, F., Gómez-Sánchez, R., et al. (2017). Conserved Atg8 recognition sites mediate Atg4 association with autophagosomal membranes and Atg8 deconjugation. EMBO Rep. *18*, 765–780.

Agrotis, A., Pengo, N., Burden, J.J., et al. (2019). Redundancy of human ATG4 protease isoforms in autophagy and LC3/GABARAP processing revealed in cells. Autophagy *15*, 976–997.

Fujita, N., Hayashi-Nishino, M., Fukumoto, H., et al. (2008a). An Atg4B mutant hampers the lipidation of LC3 paralogues and causes defects in autophagosome closure. Mol. Biol. Cell *19*, 4651–4659.

Fujita, N., Itoh, T., Omori, H., et al. (2008b). The Atg16L complex specifies the site of LC3 lipidation for membrane biogenesis in autophagy. Mol. Biol. Cell *19*, 2092–2100.

Hirata, E., Ohya, Y., and Suzuki, K. (2017). Atg4 plays an important role in efficient expansion of autophagic isolation membranes by cleaving lipidated Atg8 in Saccharomyces cerevisiae. PLoS One *12*, e0181047.

Huang, R., Xu, Y., Wan, W., et al. (2015). Deacetylation of nuclear LC3 drives autophagy initiation under starvation. Mol. Cell *57*, 456–466.

Itakura, E., Kishi-Itakura, C., and Mizushima, N. (2012). The hairpin-type tail-anchored SNARE syntaxin 17 targets to autophagosomes for fusion with endosomes/lysosomes. Cell *151*, 1256–1269.

Kabeya, Y., Mizushima, N., Ueno, T., et al. (2000). LC3, a mammalian homologue of yeast Apg8p, is localized in autophagosome membranes after processing. EMBO J. *19*, 5720–5728.

Karanasios, E., and Ktistakis, N.T. (2015). Live-cell imaging for the assessment of the dynamics of autophagosome formation: focus on early steps. Methods *75*, 54–60.

Kauffman, K.J., Yu, S., Jin, J., et al. (2018). Delipidation of mammalian Atg8-family proteins by each of the four ATG4 proteases. Autophagy *14*, 992–1010.

Kirisako, T., Ichimura, Y., Okada, H., et al. (2000). The reversible modification regulates the membrane-binding state of Apg8/Aut7 essential for autophagy and the cytoplasm to vacuole targeting pathway. J. Cell Biol. *151*, 263–276.

Koyama-Honda, I., Itakura, E., Fujiwara, T.K., et al. (2013). Temporal analysis of recruitment of mammalian ATG proteins to the autophagosome formation site. Autophagy *9*, 1491–1499.

Lamb, C.A., Yoshimori, T., and Tooze, S.A. (2013). The autophagosome: origins unknown, biogenesis complex. Nat. Rev. Mol. Cell Biol. *14*, 759–774.

Li, M., Hou, Y.F., Wang, J.S., et al. (2011). Kinetics comparisons of mammalian Atg4 homologues indicate selective preferences toward diverse Atg8 substrates. J. Biol. Chem. *286*, 7327–7338.

Liu, B., Fang, M., Hu, Y., et al. (2014). Hepatitis B virus X protein inhibits autophagic degradation by impairing lysosomal maturation. Autophagy *10*, 416–430.

Liu, P.F., Tsai, K.L., Hsu, C.J., et al. (2018). Drug repurposing screening identifies tioconazole as an ATG4 inhibitor that suppresses autophagy and sensitizes cancer cells to chemotherapy. Theranostics *8*, 830–845.

Lum, J.J., DeBerardinis, R.J., and Thompson, C.B. (2015). Autophagy in metazoans: cell survival in the land of plenty. Nat. Rev. Mol. Cell Biol. *6*, 439–448.

Mizushima, N., Yoshimori, T., and Ohsumi, Y. (2011). The role of Atg proteins in autophagosome formation. Annu. Rev. Cell Dev. Biol. *27*, 107–132.

Nair, U., Yen, W.L., Mari, M., et al. (2012). A role for Atg8–PE deconjugation in autophagosome biogenesis. Autophagy *8*, 780–793.

Nakatogawa, H., Ichimura, Y., and Ohsumi, Y. (2007). Atg8, a ubiquitin-like protein required for autophagosome formation, mediates membrane tethering and hemifusion. Cell *130*, 165–178.

Nakatogawa, H., Ishii, J., Asai, E., et al. (2012). Atg4 recycles inappropriately lipidated Atg8 to promote autophagosome biogenesis. Autophagy *8*, 177–186.

Nguyen, T.N., Padman, B.S., Usher, J., et al. (2016). Atg8 family LC3/GABARAP proteins are crucial for autophagosome–lysosome fusion but not autophagosome formation during PINK1/Parkin mitophagy and starvation. J. Cell Biol. *215*, 857–874.

Pankiv, S., Clausen, T.H., Lamark, T., et al. (2007). p62/SQSTM1 binds directly to Atg8/LC3 to facilitate degradation of ubiquitinated protein aggregates by autophagy. J. Biol. Chem. *282*, 24131–24145.

Scherz-Shouval, R., Shvets, E., Fass, E., et al. (2007). Reactive oxygen species are essential for autophagy and specifically regulate the activity of Atg4. EMBO J. *26*, 1749–1760.

Skytte-Rasmussen, M., Mouilleron, S., Kumar-Shrestha, B., et al. (2017). ATG4B contains a C-terminal LIR motif important for binding and efficient cleavage of mammalian orthologs of yeast Atg8. Autophagy *13*, 834–853.

Tsuboyama, K., Koyama-Honda, I., Sakamaki, Y., et al. (2016). The ATG conjugation systems are important for degradation of the inner autophagosomal membrane. Science *354*, 1036–1041.

Walker, S.A., and Ktistakis, N.T. (2020). Autophagosome biogenesis machinery. J. Mol. Biol. *432*, 2449–2461.

Wan, W., You, Z., Zhou, L., et al. (2018). mTORC1-regulated and HUWE1-mediated WIPI2 degradation controls autophagy flux. Mol. Cell *72*, 303–315.

Weidberg, H., Shvets, E., Shpilka, T., et al. (2010). LC3 and GATE-16/GABARAP subfamilies are both essential yet act differently in autophagosome biogenesis. EMBO J. *29*, 1792–1802.

Xie, Z.P., Nair, U., and Klionsky, D.J. (2008). Atg8 controls phagophore expansion during autophagosome formation. Mol. Biol. Cell *19*, 3290–3298.

Yoshimura, K., Shibata, M., Koike, M., et al. (2006). Effects of RNA interference of Atg4B on the limited proteolysis of LC3 in PC12 cells and expression of Atg4B in various rat tissues. Autophagy *2*, 200–208.

You, Z., Xu, Y., Wan, W., et al. (2019). TP53INP2 contributes to autophagosome formation by promoting LC3–ATG7 interaction. Autophagy *15*, 1309–1321.

Yu, L., Chen, Y., and Tooze, S.A. (2018). Autophagy pathway: cellular and molecular mechanisms. Autophagy *14*, 207–215.

Yu, Z.Q., Ni, T., Hong, B., et al. (2012). Dual roles of Atg8–PE deconjugation by Atg4 in autophagy. Autophagy *8*, 883–892.